A First Principles Study of the Vibrational Properties of Crystalline Tetracene under Pressure

Mayami Abdulla [1], Keith Refson [2,3], Richard H. Friend [1], Peter D. Haynes [4]

[1] Department of Physics, University of Cambridge, Cavendish Laboratory, 19 J. J. Thomson Avenue, Cambridge CB3 0HE, UK

[2] ISIS Facility, STFC Rutherford Appleton Laboratory, Chilton, Didcot, Oxfordshire OX11 0QX, UK

[3] Department of Physics, Royal Holloway, University of London, Egham, Surrey TW20 0EX

[4] Departments of Materials and Physics, Imperial College London, Exhibition Road, London SW7 2AZ, UK

Abstract

We present a comprehensive study of the hydrostatic pressure dependence of the vibrational properties of tetracene using periodic density-functional theory (DFT) within the local density approximation (LDA). Despite the lack of van der Waals dispersion forces in LDA we find good agreement with experiment and are able to assess the suitability of this approach for simulating conjugated organic molecular crystals. Starting from the reported X-ray structure at ambient pressure and low temperature, optimised structures at ambient pressure and under 280 MPa hydrostatic pressure were obtained and the vibrational properties calculated by the linear response method. We report the complete phonon dispersion relation for tetracene crystal and the Raman and infrared spectra at the centre of the Brillouin zone. The intermolecular modes with low frequencies exhibit high sensitivity to pressure and we report mode-specific Grüneisen parameters as well as an overall Grüneisen parameter γ=2.8. Our results suggest that the experimentally reported improvement of the photocurrent under pressure may be ascribed to an increase in intermolecular interactions as also the dielectric tensor.

1. Introduction

Organic semiconductors have great potential as active materials in optoelectronic devices. Among these materials, molecular semiconductors of the oligoacene family have attracted attention due to their promising high charge carrier mobilities, which enable them to be incorporated in functional devices such as light-emitting diodes [1, 2], field effect transistors [3-8] and photovoltaics [9-12]. The molecules within oligoacene crystals are bound together by van der Waals (vdW) dispersion forces. Therefore the crystal is compliant, so that the application of a small external pressure can significantly alter structural and electronic properties whilst preserving the chemical structure of the molecule. The interest in molecular crystals along with the pressure dependence of their properties dictates the need to correctly predict the properties of the crystal under ambient pressure conditions and when subjected to external pressure.

Density-functional theory (DFT) is by far the most popular method for performing first-principles quantum-mechanical simulations of materials, because it balances a sufficiently accurate treatment of exchange and correlation for many purposes with a moderate computational cost. However the usual approximations employed to describe exchange and correlation – the generalised gradient approximations (GGAs) – lack any account of vdW dispersion forces that play an important role in carbon-based conjugated semiconductors. Semi-empirical [13-16] and first-principles [17] descriptions of vdW interactions are under development, and the reader is advised to review Klimeš *et al.* for further information [18]. A recent DFT study performed on tetracene and other molecular crystals, and containing a correction for the vdW interactions, correctly predicts the structural, electronic and optical properties of the crystals [19, 20]. However extensions of these methods to phonon properties are not yet widely available, so for this study we return to the local density approximation

(LDA). Though it lacks a physically correct description of vdW dispersion forces, this is compensated by a tendency to overbind which usually gives fairly good predictions of equilibrium geometry in weakly-bonded molecular crystals. It might be anticipated that vibrational properties including intermolecular phonon modes may also benefit from this error cancellation, as they are defined by small perturbations around the equilibrium geometry. However this has not yet been examined in detail. It is important to emphasise that both the size of the LDA binding energy and the asymptotic behaviour are incorrect and thus its accuracy for thermochemical properties is inconsistent.

Among oligoacene crystals, tetracene ($C_{18}H_{12}$), also known as naphthacene or 2,3-benzanthracene, is a good choice for such a study due to the availability in the literature of experimental results under ambient and high pressures. Tetracene is a polycyclic aromatic hydrocarbon that consists of four fused benzene rings in a planar structure. The low temperature unit cell of polymorph-I of the crystal contains two molecules, which are arranged in herringbone layers in the *ab* plane and stacked along the *c*-axis as shown in Figure 1. The transport of charge carriers in tetracene depends upon both the internal molecular structure and the molecular packing within the crystalline state. A previous study demonstrates an increase of charge carrier mobility with pressure in tetracene, pentacene and the tetracene derivative rubrene, within the same polymorph [21, 22]. Tetracene also exhibits a sharp decrease in resistivity as the pressure increases up to 20 GPa [23]. A detailed experimental and theoretical study of the structural and vibrational properties under hydrostatic pressure revealed anisotropic changes in the lattice constants and vibrational modes [24]. Furthermore, the Raman phonon frequencies as a function of temperature and pressure were measured for the two polymorphs and the results were matched with theoretically calculated frequencies for isolated tetracene molecules [25]. All DFT studies of tetracene reported in the literature were performed using a single isolated molecule rather

than on a periodic crystal, thereby excluding the low frequency intermolecular vibrational modes that are sensitive to the change in volume and intermolecular interactions [25, 26].

This paper presents a detailed first-principles study of the tetracene molecular crystal under hydrostatic pressure. To our knowledge this is the first study of vibrational properties of an oligoacene that has been conducted on a crystal rather than a molecule. Commencing from experimentally reported X-ray structures of tetracene crystal, the properties of tetracene were calculated under ambient and 280 MPa hydrostatic pressures.

The paper is arranged as follows: Section 2 describes the computational methodology. Section 3 reports the DFT-LDA results for the structure (Sec. 3.1), phonon dispersion (Sec. 3.2), pressure dependence of the Grüneisen parameter (Sec. 3.3), Raman and infrared spectra (Sec. 3.4), and the pressure dependence of the dielectric constant (Sec. 3.5). Whenever possible, the DFT-LDA results are compared with corresponding experimental and theoretical data available in the literature. Section 4 presents the conclusions.

2. Method and Computational Details

Our calculations used the CASTEP code [27] which implements the plane-wave-pseudopotential formulation of DFT together with density-functional perturbation theory (DFPT). Exchange and correlation were treated within the LDA [28, 29]. Initially, the two available X-ray crystal structures of tetracene labelled TETCEN [30], recorded at room temperature (RT), and TETCEN01 [31], recorded at a low temperature (LT) of 175 K, available from the Cambridge Structural Database (CSD) [32] were geometry-optimised. The two structures converged to the same minimum total energy within ~6 meV per unit cell and to equivalent unit cell parameters, in agreement with reference [33]. However, the DFT-LDA phonon dispersion calculation for the RT structure resulted in imaginary frequencies for some acoustic modes, indicating the instability of this structure at 0 K. It is likely that vibrational entropy – which is not taken into account in the DFT optimisation – may stabilise this phase at RT. Accordingly, the calculations presented here proceeded using the LT structure. Figure 1 displays the crystal structure as experimentally determined at LT.

Calculations were performed on a unit cell of this tetracene crystal containing two symmetrically inequivalent molecules so that the unit cell contains a total of 36 carbon and 24 hydrogen atoms. Optimised norm-conserving pseudopotentials were used to describe the atomic nuclei and core electrons [34], and the electronic wavefunction was expanded using a plane-wave basis with cut-off energy of 780 eV. The convergence tolerance for electronic total energy minimisation was 10^{-10} eV/atom and the k-point sampling of the Brillouin zone (BZ) used a 2×2×1 mesh according to the Monkhorst-Pack (MP) scheme [35]. Unconstrained variable-cell geometry optimisations of the tetracene crystal unit cell were performed a using the Broyden–Fletcher–Goldfarb–Shanno algorithm (BFGS) [36]. As is typical for weakly bonded molecular crystals, stringent geometry optimisation convergence criteria were

required: (i) ionic forces less than 10^{-4} eV/Å; (ii) total energy change less than $5x10^{-7}$ eV/atom; and (iii) ionic displacement change less than 10^{-3} Å. The optimised structure at atmospheric pressure was then further optimised following the application of 280 MPa hydrostatic pressure to meet the same convergence criteria.

The dynamical matrix and frequencies of the harmonic phonon modes were computed using the linear response method at the Gamma (Γ) point initially and then on a 4×3×2 MP coarse grid over the BZ for the phonon crystal momentum. The coarse grid contains 14 irreducible **q**-points. The results obtained using the coarse **q**-point grid were interpolated onto a finer 18×15×9 MP grid with a total of 1,216 **q**-points to find the mode Grüneisen parameters, a very dense 35×29×17 MP grid at a total of 8,626 **q**-points for the vibrational density of states, and a fine path along high-symmetry directions in the BZ for the phonon dispersion curves defined in Ref. [37]. This Fourier interpolation method is exact under the assumption that the force constants are negligible beyond 10 Å [38]. The vibrational density of states was plotted as a weighted average over all **q**-points in the dense MP grid using Lorentzian broadening with a FWHM of 10 cm^{-1}.

Phonon dispersion curves were calculated along a path traversing the high symmetry points of the BZ defined in in the references [37, 39] and a few points in between (See Figure S1 in supplementary information).

3. Results and Discussion

3.1 Optimisation of Tetracene Structure at Ambient and 280 MPa Pressures

Table 1 presents DFT-LDA results for unconstrained optimisation of the LT structure at ambient pressure conditions together with the experimentally reported LT data [31]. In accordance with the well-known tendency of the LDA to overbind the atoms [40, 41], the volume of the DFT-LDA optimised structure at ambient pressure was smaller by ~11% than the experimentally measured volume, despite the lack of vdW forces. Upon optimisation, the lengths of all the lattice vectors decreased, with a maximum reduction in *b* of ~5%, but the cell angles did not change appreciably.

Table 1. The DFT-LDA lattice parameters for tetracene computed at ambient and 280 MPa hydrostatic pressures together with those experimentally measured in Refs. [24] and [31]. The area of the *ab* plane is defined as ($A_{ab} = ab\ sin\gamma$).

cell parameters	Ref.[31] 175K	DFT-LDA (this work)		Ref.[24], Experiment, 295K	
	1 atm	1 atm	280 MPa	1 atm	286 MPa
a/ Å	6.0565	5.8746	5.8379	6.055	6.009
b/ Å	7.8376	7.4524	7.3706	7.872	7.775
c/ Å	13.0104	12.5380	12.5095	13.42	13.36
α / °	77.127	78.091	78.332	113.39	113.27
β / °	72.118	72.152	72.037	101.10	100.39
γ / °	85.792	85.377	85.436	85.94	86.04
V/ Å^3	572.968	511.164	501.366	576	564
A_{ab} / Å^2	47.34	43.64	42.89	47.5	46.6
Z / Å	12.1	11.71	11.69	12.08	12.06

The result of compressing the optimised DFT-LDA structure at 280 MPa is shown in Table 1 along with experimental RT data under ambient and 286 MPa hydrostatic pressures reported

in Ref. [24] for comparison. Despite the substantial absolute error in the calculated lattice parameters, DFT-LDA predicts the relative changes upon compression in the volume to be ~2% in good agreement with Ref.[24]. The absolute compressions for *a* and *b* are about 20% greater than the experimentally measured values and the relative orientation of the unit cell vectors determined by the angles demonstrates very little change in both cases.

Under pressure, adjacent molecules rotate slightly and become more cofacial with an angle reduction from 71.2° to 70.6°. Consequently, the overlap between the molecular wavefunctions in the *ab* plane increases. Upon the application of a small amount of pressure, the interlayer distance Z is almost unchanged, but there is a slight increase in the angle between the planes of the adjacent molecules from 150.1° to 150.6°. This suggests that the molecules will tilt further from the *c*-axis to sustain the interlayer distance instead of slipping as suggested in Ref. [42]. Such a change of the molecular arrangement in the optimised DFT-LDA structure is in agreement with the experimental results of Ref.[24], and is also found experimentally and theoretically where other molecules adopt a herringbone structure [43-45].

3.2. Phonon Dispersion Curves

Figure 2 displays the phonon dispersion curves $\omega(q)$ computed for the two optimised structures of tetracene along a path that includes the high symmetry $\boldsymbol{q}$-points and a few others in the triclinic unit cell. There are a total of 180 branches (including three acoustic) associated with three degrees of freedom of the 60 atoms in the unit cell. The absence of imaginary modes anywhere in the BZ proves the mechanical stability of the optimised structures.

Phonon modes in molecular crystals may be classified into intramolecular and intermolecular lattice vibrations. Intermolecular modes arise from the relatively weak interactions between molecules and are characterised by low frequencies. Intramolecular modes stem from stretching and bending of the covalent bonds within the molecules, have higher frequencies, and appear in pairs (doublets) due to the presence of two inequivalent molecules within the unit cell. Previous *ab initio* calculations of isolated molecules have reported few or no modes below 300 cm^{-1} and suggest that the observed modes above ~150 cm-^{1} are solely intramolecular [25, 46, 47]. However, our periodic DFT-LDA results, which make no prior distinction between intermolecular and intramolecular modes, demonstrate that the lowest intramolecular mode is as low as 115.85 cm^{-1}. This mode has the character of slight bending of the molecule about the short molecular axis. The intermolecular and low-lying intramolecular modes shown in Figure 2 (a,b) are highly dispersive, while the higher-frequency intramolecular modes shown in Figure 2 (c,d) exhibit much less dispersion. Intramolecular modes involving atomic displacements in the molecular plane such as the modes 436.72 cm^{-1} and 438.37 cm^{-1} are almost dispersionless in all directions along the BZ. Figure 4 shows schematic illustrations of the atomic and molecular displacement associated with some of the DFT-LDA calculated phonons below 300 cm^{-1}. Further detailed information

on the displacement of atoms corresponding to each of the 180 modes is available in the supplementary information.

In general, modes are shifted to higher frequencies when tetracene is compressed, indicating that the crystal becomes stiffer. As expected, the intermolecular modes are more sensitive to the application of pressure than the intramolecular modes. The anisotropic compression of the tetracene unit cell shows that *b* decreases more than *a* and *c*. This leads to an increase in the molecular interactions within the *ab* plane and particularly along the edge-to-face intermolecular direction $\left(\overline{\Gamma K}\right)$ demonstrated by the large dispersion in some of the branches. Figure 3 compares the phonon frequencies calculated using DFT-LDA and those previously measured using inelastic neutron scattering (INS) by Pivovar et al.[24]. The results lie on a line of slope 0.98±0.01 with a correlation coefficient of 0.981 and demonstrate that DFT-LDA correctly predicts the phonon frequencies of all but a few modes. A detailed comparison of the periodic DFT-LDA phonon frequencies with those measured by Pivovar et al. [24] is presented in Table S1 in the supplementary information.

Any strong electron-phonon coupling in the low frequency intermolecular modes is of interest as this will hinder electronic transport within the crystal by modulating the probability of charge transfer between adjacent molecules. This has been observed in pentacene where a terahertz transient conductivity experiment revealed strong coupling of the charge carriers to the low frequency intermolecular modes [48, 49]. A similar effect is expected to occur in tetracene.

Figure 5 displays the vibrational density of states (VDOS) as a function of mode frequency for tetracene at ambient pressure and under 280 MPa. No major alteration arises in the VDOS upon compressing the crystal; it simply shifts under pressure towards higher frequencies.

3.3 Grüneisen Parameters

Grüneisen parameters for each phonon mode are defined by the dependence of the phonon frequencies on the crystal volume. The overall crystal Grüneisen parameter is evaluated by averaging the individual mode-Grüneisen parameters, weighted by their specific heat contributions (see supplementary information). The overall crystal Grüneisen parameter of tetracene computed by DFT-LDA is 2.82, which is 'qualitatively' similar to that measured and calculated as 3.6 and 3.46, respectively for naphthalene [50]. The BZ-averaged mode-Grüneisen parameter for modes below ~200 cm^{-1}, computed on the fine 18×15×9 MP grid of **q**-points is displayed as a function of frequency in Figure 6(a). Figure 6(b) shows the mode-Grüneisen parameters at the zone-centre for the modes below ~600 cm^{-1}. It may be seen that modes with frequency below 155 cm^{-1} are the most pressure sensitive, with Grüneisen parameters around 3, decreasing to less than 1 at higher frequencies.

3.4 Pressure Dependence of Raman and Infrared Spectra

The modes of the DFT-LDA-calculated phonons were assigned using symmetry group analysis for tetracene, $P\bar{1}\ \left(C_i^1\right)$, which predicts a total of 90 modes for each of the symmetry modes A_u and A_g respectively. The tetracene unit cell possesses a centre of symmetry; therefore, the mutual exclusion principle holds. Accordingly, the optic modes A_g and A_u are Raman active and IR sensitive respectively. The Raman and IR spectra provide information about the phonon modes only at the centre of the BZ, i.e. at **q**=0, because the incident and scattered photon wave vectors are small in contrast to the large reciprocal lattice wave vectors. Following the calculation of phonon frequencies, IR intensities were computed using DFPT and Raman activity using a hybrid numerical differentiation/DFPT method [51]. The frequencies of the low-lying Raman-active modes at ambient pressure conditions calculated using DFT-LDA plotted against the experimentally measured frequencies in Ref.[25] show excellent agreement, as indicated by the slope of (1.04±0.02) and correlation coefficient of 0.998 (see supplementary information). A small scaling error – in this case 1.04 is typical and expected of the comparison between DFT and experimental frequencies. The absence of clear deviation from the linear relationship between modes of intra- and intermolecular character supports our contention that the use of LDA to describe intermolecular interactions in molecular crystals still gives an excellent account of phonon frequencies despite its thermochemical failings. Further quantitative comparison between the frequencies of the Raman modes calculated using DFT-LDA and the previously reported results [25] is presented in Table S2 in the supplementary information.

The DFT-LDA calculated Raman spectra for the LT structure at ambient and 280 MPa pressures are depicted in Figure 7. In agreement with other high-pressure Raman studies, pressurising tetracene shifts the modes to higher frequencies. This upshift is non-uniform,

showing some variance among the mode Grüneisen parameters. Presumably this is due to the influence of the anisotropic compression of the unit cell vectors on the specific mode eigenvectors. Figure 7 also shows that both the intensity and the frequency of the modes increase with pressure. In contrast to the excellent agreement of frequency data, there is some discrepancy between the computed Raman intensities of Figure 7 with the experimental LT spectrum in Figure 1 of Ref. [25]. However, Figure 7 does show three closely-spaced Raman bands computed at ambient pressure at 53.8 cm^{-1}, 61.4 cm^{-1}, and 73.2 cm^{-1} in agreement with the experimentally reported spectrum.

The calculated IR frequencies corresponding to selected phonon modes are presented and compared with experimental and theoretical data from the literature in Table 2 [52-56]. In general, the frequencies calculated here are in good agreement with the previous representative data. This work additionally predicts several bands in the intermolecular low frequency region below 160 cm^{-1}. These are not present in the single molecule case and have not been experimentally observed, either due to limitation of the techniques used in measurements or their very low intensity.

The infrared spectrum computed with DFT-LDA at the centre of the BZ for modes with frequencies below 400 cm^{-1} are depicted in Figure 8 for the LT structure at ambient pressure and at 280 MPa. Broad bands appear in the IR spectrum due to close proximity of the modes, just as in the Raman spectrum. Upon the application of pressure, there is a blue-shift in frequency accompanied by a change in intensity. Complete information about the DFT-LDA calculated phonon modes including their assignment to Raman and infrared modes and with their associated intensities is available in the supplementary information.

Table 2. Comparison of the frequencies of the intermolecular and some of the intramolecular infrared modes (in cm^{-1}) calculated using DFT-LDA (this work) and reported experimental and theoretically calculated data from literature [52-56]. *R* denotes predicted Raman-active band.For complete infrared DFT-LDA calculated modes see supplementary information.

This work	Ref.[52, 56]		Ref. [55]	Ref. [53, 54]	
	Expt.	calc.	calc.	Expt.	calc.
41.6					
74.4					
80.4					
115.8	106				
117.5					
146.7					
157.4					
169.2	166	166	160		
177.3					
272.4	271	278	266		
280.3					
329.1					
332.3					
436.7	390	388	374*R*		
438.4					
460.2	459	485	464		465.1
476.1	469	492	472		473.5
483.1					
491.5					
553.8	550	574	556		555.7
557.5					
569.0					
574.2	572	578	561*R*		
612.0	607	631	611	607.7	610.9
614.0					
628.1	626	662	640	627.7	640.2
628.4					
728.8	655		735		735.4
748.8	740	774	746	740.5/ 742.9	747.2
758.9	753	780*R*	754*R*		
760.4	784	800*R*	763*R*	766.7	
769.5					
773.4					
831.3	836	870*R*	833*R*		
834.7			841*R*		
888.8	881	927*R*	884*R*		
889.9			899*R*		
908.7	904	943	905	895.3	906.3
909.8					
928.3	931	965	935	933.4	935.6
928.9					
957.9					
960.1	971	999	961	953.6/ 956	961.6
979.4				964.7	
987.6					
1011.4	995	1025	996	997	995.8

3.5 Pressure Dependence of Dielectric Constant

The propagation of radiation through the crystal subject to a low-frequency (*IR* and lower) external electric field is described by the static dielectric tensor (ε_0) whilst the optical (electronic) tensor (ε_∞) describes the interaction of the crystal with a high-frequency electric field. The frequency-dependent dielectric function $\varepsilon(\omega)$ depends on the electronic polarisability, Born effective charges, and phonon frequencies and was evaluated from these DPFT-computed quantities. Table 3 presents the complete dielectric tensors as well as their principal values for tetracene calculated at ambient pressure and 280 MPa. Because of the triclinic symmetry of the tetracene crystal, both the static and optical dielectric tensors are anisotropic with three distinct diagonal components ε_{xx} , ε_{yy} and ε_{zz} . The DFT-LDA calculated optical dielectric constant at ambient pressure is higher than the experimentally reported values due to the underestimation of the band gap, which is inversely proportional to $\varepsilon(\omega)$ [57, 58]. It increases as the crystal is compressed. The pressure dependence of $\varepsilon(\omega)$, expressed as a dielectric Grüneisen parameter $\gamma^{\varepsilon} = \frac{-d\ln(\varepsilon)}{d\ln(V)}$, is shown in Table 3. This shows that $\varepsilon(\omega)$ is sensitive to the change that occurs along the *b* direction within the *ab* herringbone plane in the unit cell rather than along the *c* direction of the stacking layers. The sensitivity of $\varepsilon(\omega)$ is signified by the large values of the Grüneisen parameter for both the optical and static dielectric constants.

DFT-LDA calculations of the band structure at ambient and high pressures are shown in the supplementary information. There is a direct band gap of 1.03 eV located at the principal symmetry point **K** (0.5,0.5,0), similar to that reported using DFT-GGA [39], but lower than the experimentally measured optical gap at room temperature and ambient pressure of 2.3 eV [59, 60]. This decreases under pressure to 0.96 eV. Compression increases the π-π coupling between molecules in the ***ab****** plane as signified by the increase in the frequency of the

intermolecular phonons, in turn increasing the transfer integral and the rate of charge transfer in the compressed tetracene relative to that at ambient pressure. The increase in the transfer integral is accompanied by the increase of the bandwidth of the HOMO and LUMO leading to a reduction in the band gap. Furthermore, the increase in the transfer integral leads to an increase in the mobility of charge carriers in accord with the experimental observation [21]. Hence, DFT-LDA data suggest that the increase in the photocurrent under the application of pressure reported in Ref. [21] is due to both the improvement in mobility resulting from the increase of overlap of molecular wavefunctions in the ***ab**** plane and the associated increase in the transfer integral, and to the increase of the photogenerated charge facilitated by the increase of the dielectric constant [23, 61, 62].

Table 3: The complete dielectric tensor together with the eigenvalues for the optical frequencies ($\omega\to\infty$) and the low frequencies ($\omega\to 0$) for DFT-LDA optimised LT tetracene structure at ambient and 280MPa pressures. Also the dielectric Grüneisen parameter is shown. The Cartesian *x*-axis is taken to be along the crystal *x*-direction parallel to the lattice vector *a*.

		($\omega\to\infty$)			($\omega\to 0$)		
		x	*y*	*z*	*x*	*y*	*z*
1 atm	*x*	3.99	0.24	-0.60	4.12	0.24	-0.57
	y	0.24	3.26	-0.86	0.24	3.55	-0.78
	z	-0.60	-0.86	5.41	-0.57	-0.78	5.52
eigenvalues		5.93, 3.78, 2.96			5.99, 3.92, 3.28		
280 MPa	*x*	4.10	0.25	-0.60	4.23	0.24	-0.57
	y	0.25	3.38	-0.89	0.24	3.68	-0.81
	z	-0.60	-0.89	5.54	-0.57	-0.81	5.66
eigenvalues		6.08, 3.89, 3.06			6.15, 4.04, 3.39		
		ε_{xx}	ε_{yy}	ε_{zz}	ε_{xx}	ε_{yy}	ε_{zz}
γ_{ε}		1.53	2.11	1.36	1.54	2.04	1.41

4. Conclusions

The applicability of DFT-LDA to probe the pressure dependence of structural and vibrational properties of organic molecular crystals has been assessed through the calculation of tetracene properties. In spite of the lack of account of vdW dispersion forces and the tendency of DFT-LDA to overbind atoms, resulting in smaller calculated volumes than found in experiment, there is good agreement for the vibrational properties and associated Raman and infrared spectra between theory and experiment. For the first time, the complete set of phonon dispersion relations have been presented for tetracene enabling computation of the Grüneisen parameter. As indicated by the mode-specific Grüneisen parameters, the intermolecular modes were more sensitive to the applied pressure than the intramolecular modes as expected. The DFT-LDA of a unit cell of tetracene crystal utilising equal treatment for intermolecular and intramolecular modes calculates the lowest intramolecular mode to be as low as 115.85 cm^{-1} which is lower than the previously reported lowest intramolecular mode 146.5 cm^{-1} from a single isolated molecule calculation. The DFT-LDA results also reveal that application of hydrostatic pressure increases the dielectric tensors anisotropically with a maximum change exhibited along the *b* axis. Therefore, these results suggest that the experimentally reported improvement of the photocurrent under pressure may be ascribed to the increase of the intermolecular interactions as well as the dielectric tensor.

Acknowledgments

The authors acknowledge the use of University of Cambridge High Performance Computing Service and the computational resources on HECToR funded by EPSRC Grant EP/F038356/1. M. Abdulla thanks the University of Bahrain for financial support.

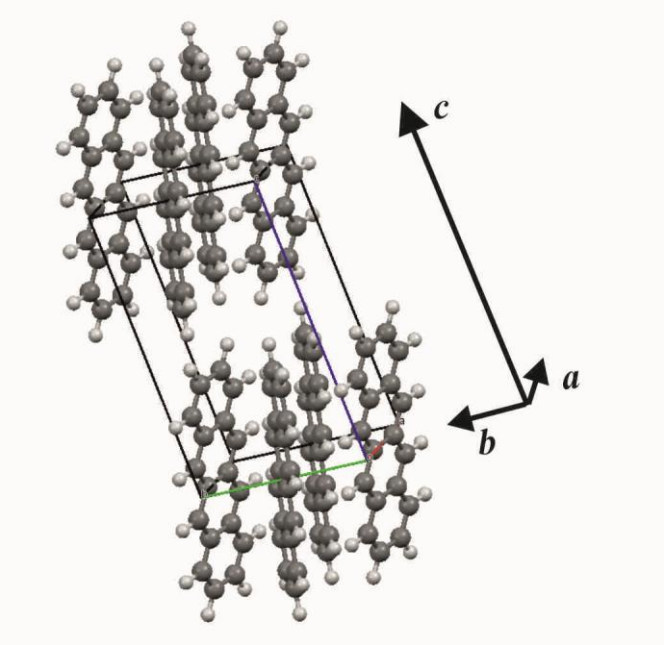

Figure 1. The structure of tetracene crystal at ambient pressure and a temperature of 175K. The image illustrates the stacking of the layers along the *c*-axis.

.

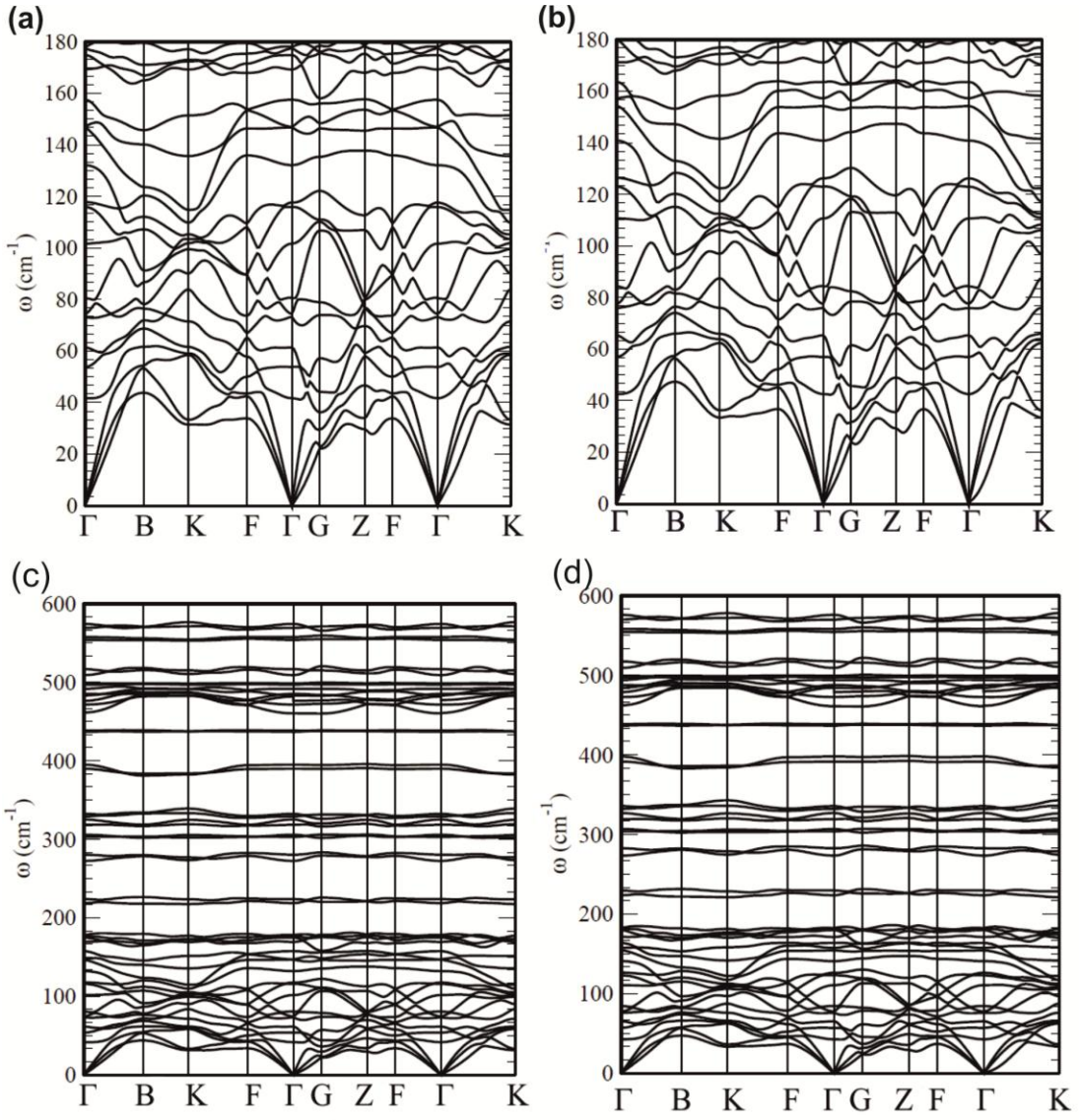

Figure 2. Theoretically DFT-LDA calculated dispersion relations for LT tetracene along the principal symmetry directions and some other points in BZ along the path described in Figure 2. The intermolecular modes in (a) and (b) are at ambient pressure and under hydrostatic pressure of 280MPa, respectively. The intermolecular and low-laying intramolecular modes in (c) and (d) are at ambient pressure and under hydrostatic pressure of 280MPa, respectively. The high symmetry points of the BZ are labelled relative to the cell vectors according to reference [37].

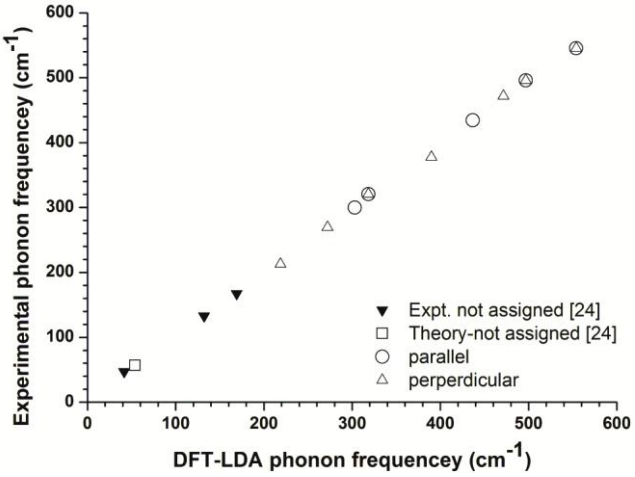

Figure3**.** Correspondence between theoretically DFT-LDA calculated and experimentally measured INS phonons' frequencies reported in reference [24] at ambient pressure for tetracene crystal. Parallel and perpendicular refers to the atomic displacement with respect to the molecular plane.

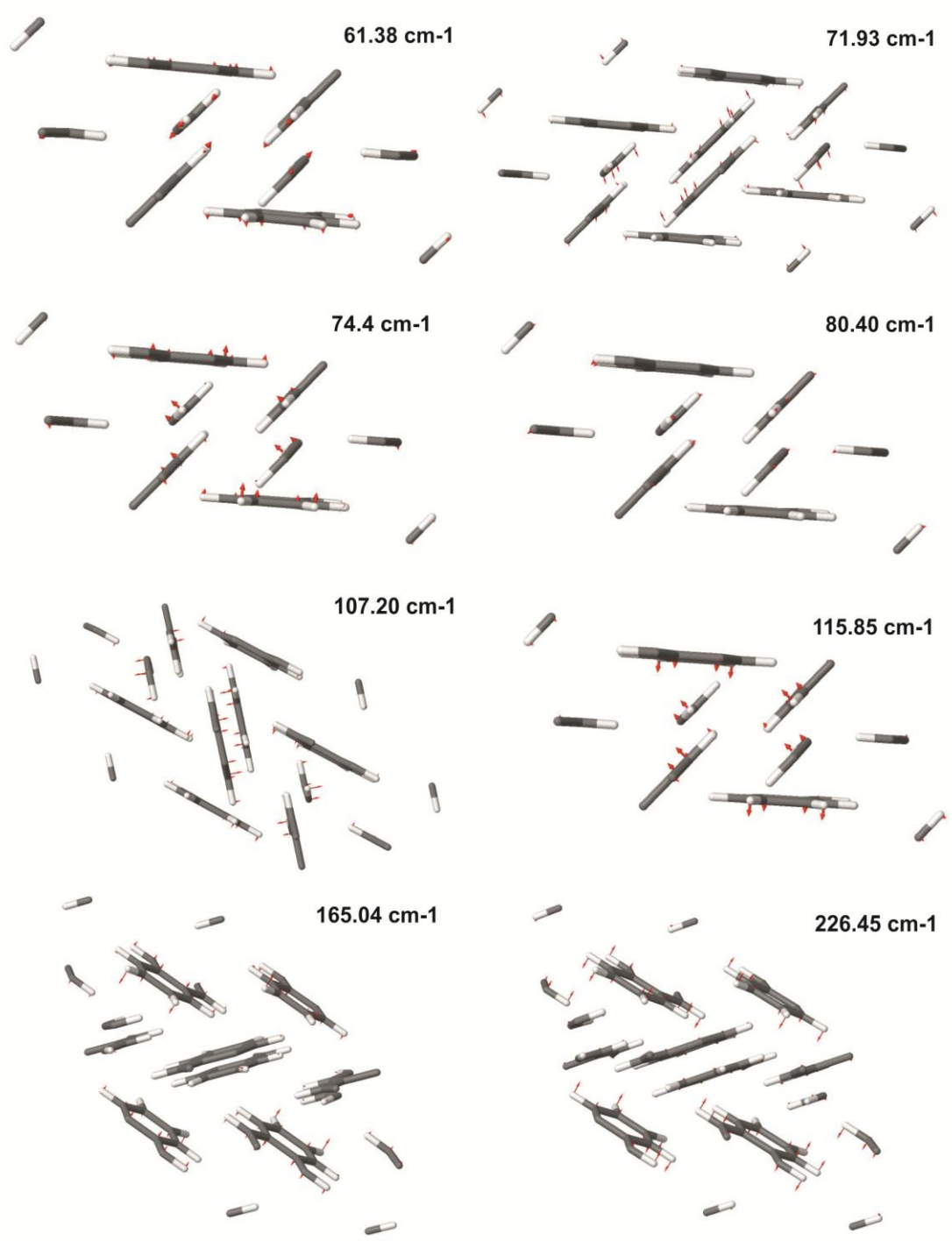

Figure4. The atomic displacements for some DFT-LDA calculated modes at the zone-centre of BZ for LT tetracene. The length of the vector is associated with the magnitude of the displacement amplitude. (1cm-1~0.125 meV).

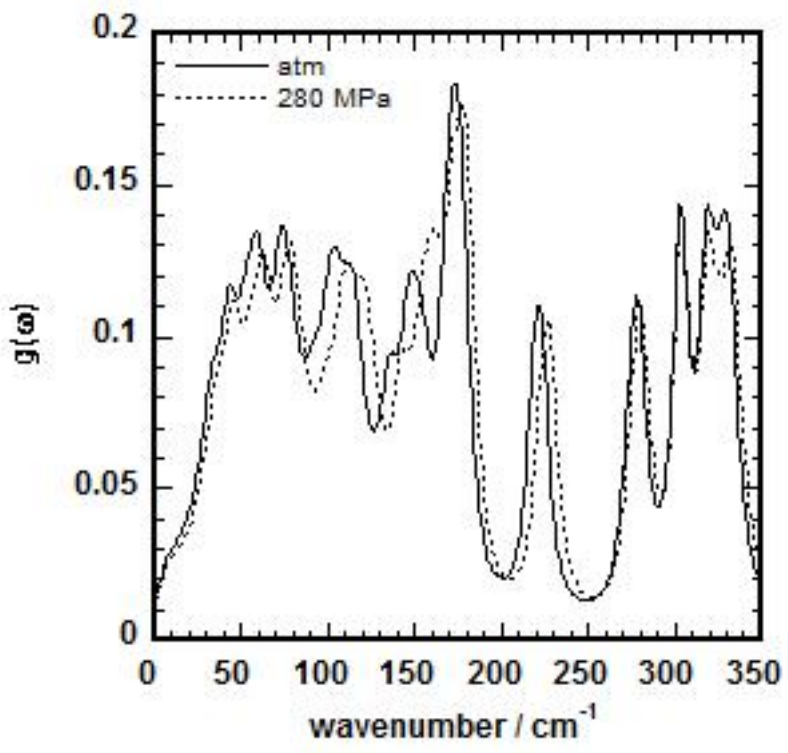

Figure 5. Theoretically DFT-LDA calculated vibrational density of states for LT tetracene at ambient pressure and under hydrostatic pressure of 280MPa.

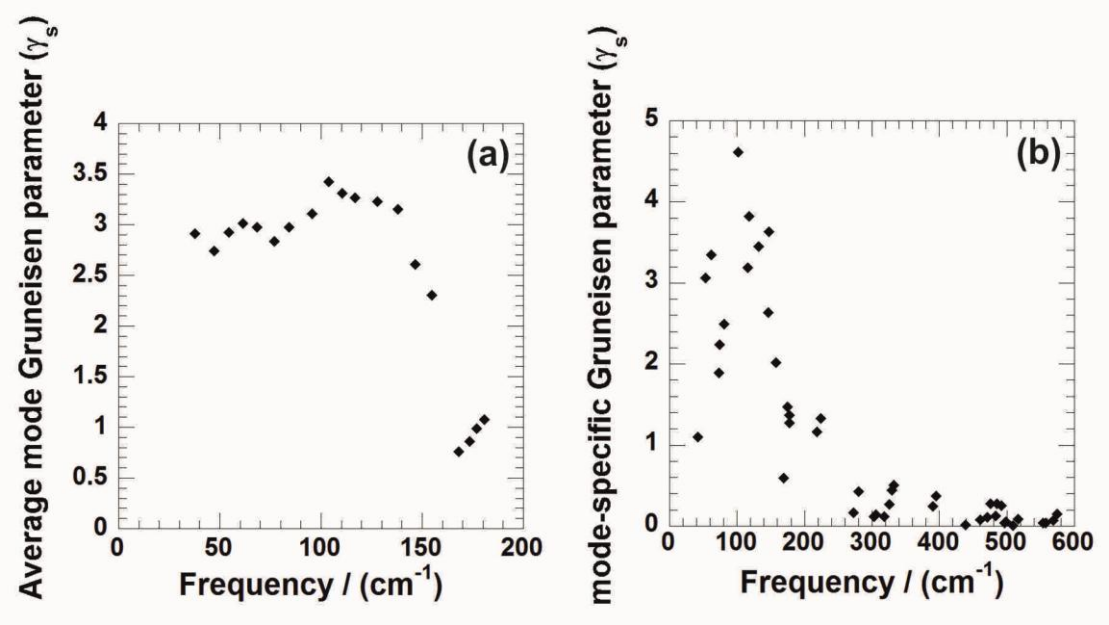

Figure 6. (a) The average mode-specific Grüneisen parameter of tetracene crystal as a function of mode frequency for the intermolecular low frequency modes. (b) The mode-specific Grüneisen parameter of tetracene crystal at Γ as a function of mode frequency for the modes with frequencies below 600 cm^{-1}.

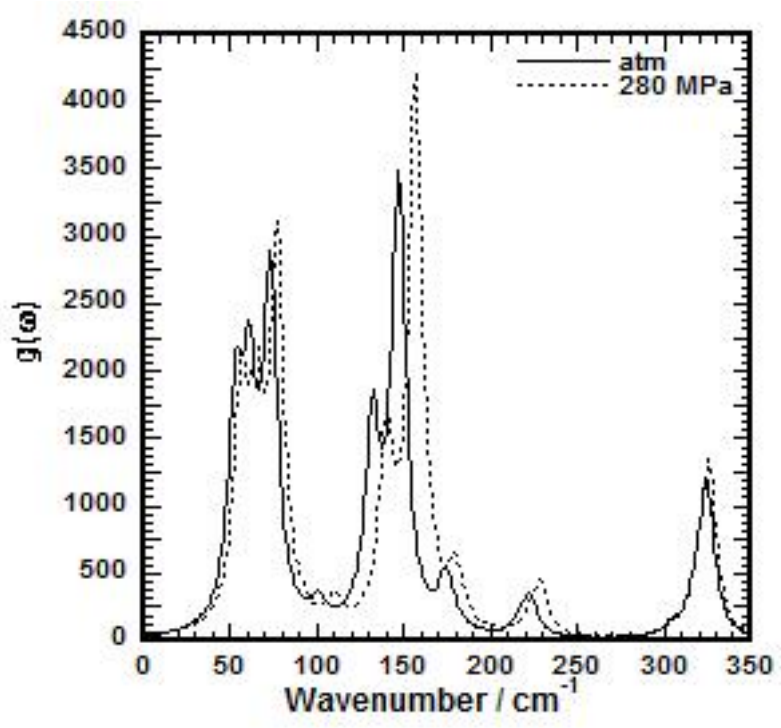

Figure 7. The Raman spectra of LT tetracene structure at ambient pressure conditions (solid line) and under hydrostatic pressure of 280MPa (dotted line).

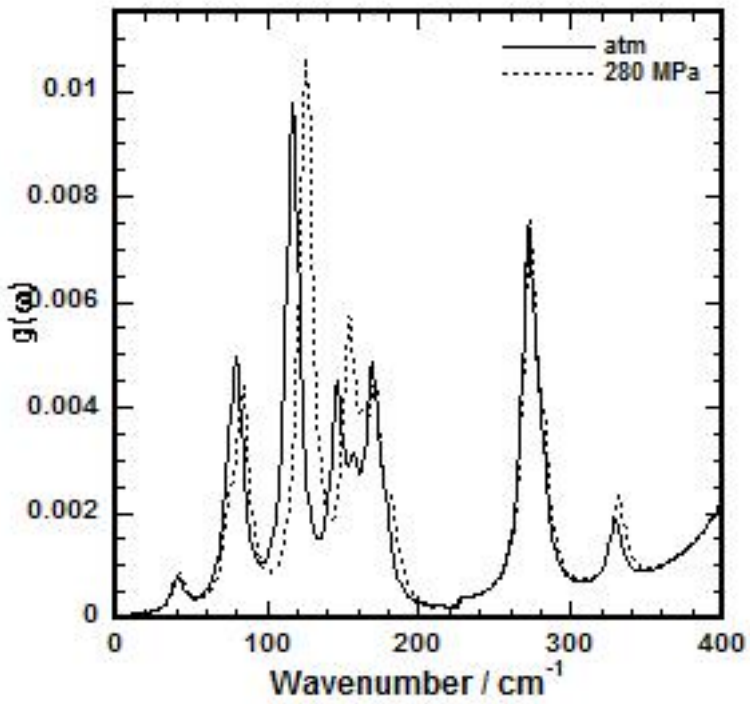

Figure 8. The infrared spectra of LT tetracene structure at ambient pressure conditions and under hydrostatic pressure of 280MPa.

References

1. Choi, H.J.P., Young Wook; Choi, Jin Hwan; Park, Tae Hyun; Song, Eun Ho; Ju, Byeong Kwon. *Improved electroluminescent efficiency of OLEDs by pentacene as HIL/HTL and plasma treatment on ITO anode.* in *10th International Meeting on Information Display and International Display Manufacturing Conference and Asia Display (IMID/IDMC/ASIA Display)*. 2010. Seoul, Korea.
2. Zhang, F., et al., *Improved performance of organic light emitting diodes by pentacene as hole transporting layer.* Applied Surface Science, 2008. **255**(5(1)): p. 1942-1945.
3. Klauk, H., et al., *High-mobility polymer gate dielectric pentacene thin film transistors.* Journal of Applied Physics, 2002. **92**(9): p. 5259-5263.
4. Fang-Chung, C. and et al., *Morphological study on pentacene thin-film transistors: the influence of grain boundary on the electrical properties.* Journal of Physics D: Applied Physics, 2010. **43**(40): p. 405103.
5. Choi, J.-M., et al., *Comparative study of the photoresponse from tetracene-based and pentacene-based thin-film transistors.* Applied Physics Letters, 2006. **88**(4): p. 043508-3.
6. Gundlach, D.J., et al., *Thin-film transistors based on well-ordered thermally evaporated naphthacene films.* Applied Physics Letters, 2002. **80**(16): p. 2925-2927.
7. Yun, D.-J. and S.-W. Rhee, *Pentacene Thin-Film Transistor with NiO_x as a Source/Drain Electrode Deposited with Sputtering.* Journal of The Electrochemical Society, 2008. **155**(11): p. H899-H902.
8. Santato, C., F. Cicoira, and S. Bertolazzi, *Tetracene films for light-emitting transistors: chemical and physical effects of the organic dielectric substrates.* American Physical Society, 2010(APS March Meeting 2010, March 15-19).
9. Nolasco, J.C., et al., *Relation between the barrier interface and the built-in potential in pentacene/C_{60} solar cell.* Applied Physics Letters, 2010. **97**(1): p. 013305-3.
10. Shao, Y., et al., *Enhancement of tetracene photovoltaic devices with heat treatment.* Applied Physics Letters, 2007. **90**(10): p. 103501-3.
11. Dissanayake, D.M.N.M., et al., *Charge transfer between acenes and PbS nanocrystals.* Nanotechnology, 2009. **20**(19): p. 195205.
12. Ehrler, B., et al., *In situ measurement of exciton energy in hybrid singlet-fission solar cells.* Nat Commun, 2012. **3**: p. 1019.
13. Ortmann, F., F. Bechstedt, and W.G. Schmidt, *Semiempirical van der Waals correction to the density functional description of solids and molecular structures.* Physical Review B, 2006. **73**(20): p. 205101.
14. Grimme, S., *Semiempirical GGA-type density functional constructed with a long-range dispersion correction.* Journal of Computational Chemistry, 2006. **27**(15): p. 1787-1799.
15. Jurečka, P., et al., *Density functional theory augmented with an empirical dispersion term. Interaction energies and geometries of 80 noncovalent complexes compared with ab initio quantum mechanics calculations.* Journal of Computational Chemistry, 2007. **28**(2): p. 555-569.
16. Tkatchenko, A. and M. Scheffler, *Accurate Molecular Van Der Waals Interactions from Ground-State Electron Density and Free-Atom Reference Data.* Physical Review Letters, 2009. **102**(7): p. 073005.
17. Dion, M., et al., *Van der Waals Density Functional for General Geometries.* Physical Review Letters, 2004. **92**(24): p. 246401.
18. Klimeš, J. and A. Michaelides, *Perspective: Advances and challenges in treating van der Waals dispersion forces in density functional theory.* The Journal of Chemical Physics, 2012. **137**(12): p. 120901(1-12).
19. Schatschneider, B., et al., *Understanding the structure and electronic properties of molecular crystals under pressure: Application of dispersion corrected DFT to oligoacenes.* Journal of Physical Chemistry A, 2013. **117**(34): p. 8323-8331.

20. Reilly, A.M. and A. Tkatchenko, *Understanding the role of vibrations, exact exchange, and many-body van der Waals interactions in the cohesive properties of molecular crystals.* Journal of Chemical Physics, 2013. **139**(2).
21. Rang, Z., et al., *Hydrostatic-pressure dependence of the photoconductivity of single-crystal pentacene and tetracene.* Applied Physics Letters, 2001. **79**(17): p. 2731-2733.
22. Zhenlin, R., et al., *Hydrostatic pressure dependence of charge carrier transport in single-crystal rubrene devices.* Applied Physics Letters, 2005. **86**(12): p. 123501.
23. Samara, G.A. and H.G. Drickamer, *Effect of pressure on the resistance of fused-ring aromatic compounds.* The Journal of Chemical Physics, 1962. **37**(3): p. 474-479.
24. Pivovar, A.M., et al., *Structural and vibrational characterization of the organic semiconductor tetracene as a function of pressure and temperature.* Chemical Physics, 2006. **325**(1): p. 138-151.
25. Venuti, E., et al., *Phonons and structures of tetracene polymorphs at low temperature and high pressure.* Physical Review B, 2004. **70**(10): p. 104106.
26. Brillante, A., et al., *Raman phonon spectra of pentacene polymorphs.* Chemical Physics Letters, 2002. **357**(1–2): p. 32-36.
27. Clark, S.J., et al., *First principles methods using CASTEP.* Zeitschrift fuer Kristallographie, 2005. **220**(5-6-2005): p. 567-570.
28. Perdew, J.P. and A. Zunger, *Self-interaction correction to density-functional approximations for many-electron systems.* Physical Review B, 1981. **23**(10): p. 5048-5079.
29. Ceperley, D.M. and B.J. Alder, *Ground State of the Electron Gas by a Stochastic Method.* Physical Review Letters, 1980. **45**(7): p. 566-569.
30. Campbell, R.B., J.M. Robertson, and J. Trotter, *The crystal structure of hexacene, and a revision of the crystallographic data for tetracene.* Acta Crystallographica, 1962. **15**: p. 289-290
31. Holmes, D., et al., *On the nature of nonplanarity in the [N]Phenylenes.* Chemistry – A European Journal, 1999. **5**(11): p. 3399-3412.
32. Allen, F.H., *The Cambridge Structural Database: A quarter of a million crystal structures and rising.* Acta Crystallographica Section B: Structural Science, 2002. **58**(3 PART 1): p. 380-388.
33. Della Valle, R.G., et al., *Inherent structures of crystalline tetracene.* The Journal of Physical Chemistry A, 2006. **110**(37): p. 10858-10862.
34. Rappe, A.M., et al., *Optimized pseudopotentials.* Physical Review B, 1990. **41**(2): p. 1227-1230.
35. Monkhorst, H.J. and J.D. Pack, *Special points for Brillouin-zone integrations.* Physical Review B, 1976. **13**(12): p. 5188.
36. Pfrommer, B.G., et al., *Relaxation of Crystals with the Quasi-Newton Method.* Journal of Computational Physics, 1997. **131**(1): p. 233-240.
37. Bradley, C.J. and A.P. Cracknell, *Mathematical theory of symmetry in solids: representation theory for point groups and space groups* 1972 Oxford: Oxford University Press.
38. Refson, K., P.R. Tulip, and S.J. Clark, *Variational density-functional perturbation theory for dielectrics and lattice dynamics.* Physical Review B, 2006. **73**(15): p. 155114.
39. Hummer, K. and C. Ambrosch-Draxl, *Electronic properties of oligoacenes from first principles.* Physical Review B, 2005. **72**(20): p. 205205.
40. Mazzone, A.M., *Systematic ab initio study of the electronic properties of different pure and mixed systems formed by Cu and Ag.* Computational Materials Science, 2002. **25**(3): p. 353-362.
41. van de Walle, A. and G. Ceder, *Correcting overbinding in local-density-approximation calculations.* Physical Review B, 1999. **59**(23): p. 14992.
42. Sondermann, U., A. Kutoglu, and H. Bassler, *X-ray diffraction study of the phase transition in crystalline tetracene.* The Journal of Physical Chemistry, 1985. **89**(9): p. 1735-1741.

43. Heimel, G. and et al., *Chain-length-dependent intermolecular packing in polyphenylenes: a high pressure study.* Journal of Physics: Condensed Matter, 2003. **15**(20): p. 3375.
44. Oehzelt, M., et al., *Crystal structure of oligoacenes under high pressure.* Physical Review B, 2006. **74**(10): p. 104103.
45. Hummer, K., P. Puschnig, and C. Ambrosch-Draxl, *Ab initio study of anthracene under high pressure.* Physical Review B, 2003. **67**(18): p. 184105.
46. Weinberg-Wolf, J.R., et al., *Evidence of low intermolecular coupling in rubrene single crystals by Raman scattering.* Journal of Physics: Condensed Matter, 2007. **19**(27): p. 276204.
47. Yamakita, Y., J. Kimura, and K. Ohno, *Molecular vibrations of [n]oligoacenes (n=2−5 and 10) and phonon dispersion relations of polyacene.* The Journal of Chemical Physics, 2007. **126**(6): p. 064904(1-15).
48. Laarhoven, H.A.v., et al., *On the mechanism of charge transport in pentacene.* The Journal of Chemical Physics, 2008. **129**: p. 044704.
49. Troisi, A., *Charge transport in high mobility molecular semiconductors: classical models and new theories.* Chemical Society Reviews, 2011. **40**(5): p. 2347-2358.
50. Wang, L.J., Q.K. Li, and Z. Shuai, *Effects of pressure and temperature on the carrier transports in organic crystal: A first-principles study.* The Journal of Chemical Physics, 2008. **128**(19): p. 194706.
51. Porezag, D. and M.R. Pederson, *Infrared intensities and Raman-scattering activities within density-functional theory.* Physical Review B, 1996. **54**(11): p. 7830-7836.
52. Michaelian, K.H., et al., *Far-infrared photoacoustic spectra of tetracene, pentacene, perylene and pyrene.* Vibrational Spectroscopy, 2009. **49**(1): p. 28-31.
53. Hudgins, D.M. and S.A. Sandford, *Infrared spectroscopy of matrix isolated polycyclic aromatic hydrocarbons. 1. PAHs containing two to four rings.* The Journal of Physical Chemistry A, 1998. **102**(2): p. 329-343.
54. Langhoff, S.R., *Theoretical infrared spectra for polycyclic aromatic hydrocarbon neutrals, cations, and anions.* The Journal of Physical Chemistry, 1996. **100**(8): p. 2819-2841.
55. Malloci, G., C. Joblin, and G. Mulas, *On-line database of the spectral properties of polycyclic aromatic hydrocarbons.* Chemical Physics, 2007. **332**(2-3): p. 353-359.
56. Michaelian, K.H., et al., *Far- and mid-infrared photoacoustic spectra of tetracene, pentacene, perylene and pyrene.* Vibrational Spectroscopy, 2012. **58**(0): p. 50-56.
57. Sebastian, L., G. Weiser, and H. Bässler, *Charge transfer transitions in solid tetracene and pentacene studied by electroabsorption.* Chemical Physics, 1981. **61**(1–2): p. 125-135.
58. Bounds, P.J., et al., *Calculation and spectroscopic assignment of charge-transfer states in solid anthracene, tetracene and pentacene.* Chemical Physics, 1985. **95**(2): p. 197-212.
59. Hummer, K. and C. Ambrosch-Draxl, *Oligoacene exciton binding energies: Their dependence on molecular size.* Physical Review B, 2005. **71**(8): p. 081202.
60. Jeong, M.C., et al., *Comparative study of the photoresponse from tetracene-based and pentacene-based thin-film transistors.* Applied Physics Letters, 2006. **88**(4): p. 043508.
61. Albert-Seifried, S., et al., *Pressure-induced delocalization of photoexcited states in a semiconducting polymer.* Physical Review Letters, 2011. **105**(19): p. 195501.
62. Abdulla, M., *Experimental and Theoretical Study of Conjugated Polymers and a Molecular Crystal*, in *Physics*. 2012, University of Cambridge: UK.